JACS
JOURNAL OF THE AMERICAN CHEMICAL SOCIETY
Article
pubs.acs.org/JACS

Field Effects Induce Bathochromic Shifts in Xanthene Dyes

Martha Sibrian-Vazquez,[†] Jorge O. Escobedo,[†] Mark Lowry,[†] Frank R. Fronczek,[‡] and Robert M. Strongin*,[†]

[†]Department of Chemistry, Portland State University, 1719 SW 10th Ave., Portland, Oregon 97201, United States
[‡]Department of Chemistry, Louisiana State University, 232 Choppin Hall, Baton Rouge, Louisiana 70803, United States

Supporting Information

ABSTRACT: There is ongoing interest in near-infrared (NIR) absorbing and emitting dyes for a variety of biomedical and materials applications. Simple and efficient synthetic procedures enable the judicious tuning of through-space polar (field) effects as well as low barrier hydrogen bonding to modulate the HOMO−LUMO gap in xanthene dyes. This affords unique NIR-absorbing xanthene chromophores.

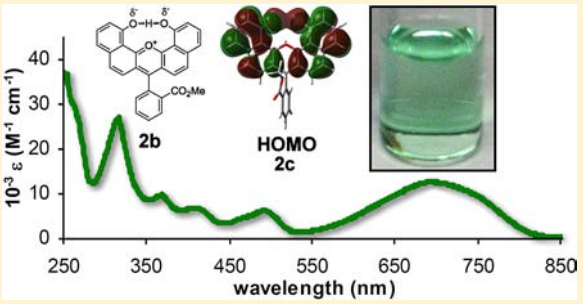

INTRODUCTION

Near-infrared (NIR) dyes are of great interest in biomedicine due to diminished interfering absorption and fluorescence from biological samples, inexpensive laser diode excitation, reduced scattering, and enhanced tissue penetration depth.[1] However, only one NIR probe, indocyanine green (ICG), is approved by the FDA.[2] ICG is challenging to use for many applications due to its amphiphilicity and limited functionalizability. Moreover, it displays high affinity for proteins with concomitant quenching upon binding.[3] It displays a small Stokes shift and low quantum yield and is known to dimerize in aqueous solution at low concentrations, which further lowers its quantum yield.[4] Designing alternatives to ICG is thus an ongoing goal.

Several halogenated and nonhalogenated xanthene dyes are sufficiently nontoxic to be used as food dyes.[5] However, xanthene dyes typically possess small Stokes shifts and are not active in the NIR. Thus, strategies for red-shifting xanthene dyes for biodiagnostics and imaging applications have been an active area of investigation for many years. Strategies employed have included replacement of the phenyl ring with electron withdrawing groups such as cyano or trifluoromehtyl,[6] extending the π-conjugation,[7] replacement of the bridging O-atom by tetrahedral carbon,[8] and annulation.[9] As a result, there are currently a large number of excellent long wavelength xanthene-based dyes. They mainly find utility in cellular imaging applications, as their spectral properties are outside the useful NIR (ca. 700−800 nm) range.

In 2008, it was demonstrated that, when an internal xanthene ether oxygen is replaced with a dimethylsilyl moiety, a bathochromic shift of 90 nm is obtained.[10] This is due to the well-known polar effect of heavy atoms on the HOMO−LUMO energy gap observed in many related classes of chromophores.[11] This useful design concept has been recently applied to other scaffolds including anthracene,[12] fluorescein,[13] and a variety rhodamine derivatives.[14] Si-rhodamines with NIR emission as great as 740 nm have been created. However, their Stokes shifts are typically less than 20 nm and they are obtained in low overall yields from multistep procedures.[14d]

Experimentally observable intramolecular Coulombic interactions resulting from direct action through space rather than through bonds are known as field effects.[15] In 2008, we reported that altering the known regiochemical functionalization of annulated xanthene dyes led to large (>100 nm) Stokes shifts and NIR emission.[16] This prior study has led us to propose that, by tuning through-space interactions of polar groups (field effects)[15] in the xanthene ring system, one could also favorably alter the electronic properties of the chromophore.

Benzannulated xanthenes typically possess polar groups on C-3 and C-11, as in **1** or C-3 and C-10 as in **3** (Figure 1). Positioning polar groups on C-1 and C-10 (as in **4**) or C-1 and C-13 (as in **2**) can potentially modulate the HOMO−LUMO gap. This embodies a relatively facile means to reduce the energy gap without the need to replace the internal oxygen with heavy atoms.

RESULTS AND DISCUSSION

Synthesis of Symmetric and Asymmetric Naphthoxanthenes. To test this hypothesis, a series of symmetric and asymmetric naphthoxanthenes **1**−**4** were synthesized and evaluated. Naphthofluorescein **1a** is commercially available. Known SNAFL-1 (herein **3a**) was prepared as previously reported.[9b] The rest of the symmetric and asymmetric naphthoxantene fluorophores were synthesized by condensation of 1,8-dihydroxynaphthalene with phthalic anhydride, 3,5-

Received: March 16, 2012
Published: May 29, 2012

dx.doi.org/10.1021/ja302445w | J. Am. Chem. Soc. 2012, 134, 10502−10508

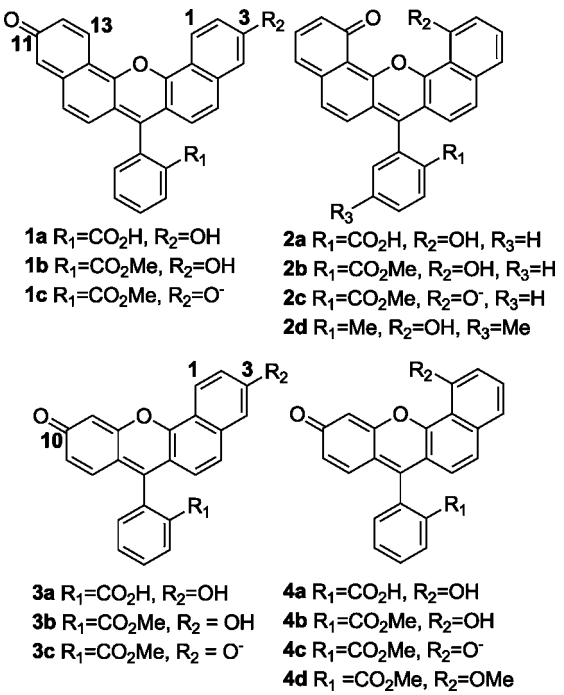

Figure 1. Structures of benzannulated xanthenes.

dimethylbenzaldehyde, and 2-(2,4-dihydroxybenzoyl)benzoic acid respectively using a mixture of CH_3SO_3H:TFA 1:1 at 80 °C for 16−24 h. The corresponding methyl ester derivatives were obtained by Fischer esterification in MeOH catalyzed by H_2SO_4; further methyl alkylation was furnished by treatment of either the carboxylate or methyl ester intermediate with methyl iodide in the presence of K_2CO_3 in DMF. The required 1,8-dihydroxynaphthalene and 2-(2,4-dihydroxybenzoyl)-benzoic acid derivatives were synthesized according to described or modified literature protocols.[9a,16,17] All compounds were isolated by flash column chromatography and characterized by NMR and MS. The structure of **4a** as the lactone form (Figure S1 of the Supporting Information) was also confirmed by X-ray single crystal structure. The target compounds were obtained in overall yields ranging from 17 to 86% as described in the Supporting Information.

Spectroscopic Characterization. The study of **1a**−**4a** in MeOH, DMSO and aqueous acid is complicated by the carboxylate-lactone equilibrium. (Figures S27−30 and Scheme S2 of the Supporting Information) This prompted us to focus our initial investigations on esters **1b**−**4b** and their corresponding anions **1c**−**4c**. It is noteworthy, however, that **2a** exists as the corresponding colorless lactone in 1:9 DMSO:buffer below physiological pH of 7.4. It thus embodies a unique pH probe, in stark contrast to known intracellular pH sensors[18] such as **1a** and congeners that generally function as turn-on indicators above pH 5 (Figure S29 of the Supporting Information).

Part a of Figure 2 displays the absorption spectra and a room light photograph of **1b**−**4b** in MeOH. A summary of the experimental and calculated absorption, and emission maxima values are given in Table 1. The placement of R_2 proximal to the xanthene internal oxygen in **2b** and **4b** affords bathochromic shifts of 103 and 15 nm as compared to **1b** and **3b**, respectively. The formal transposition of R_2 also imparts similar corresponding shifts in the excitation spectra (part b of Figure 2) and large bathochromic shifts in the fluorescence emission

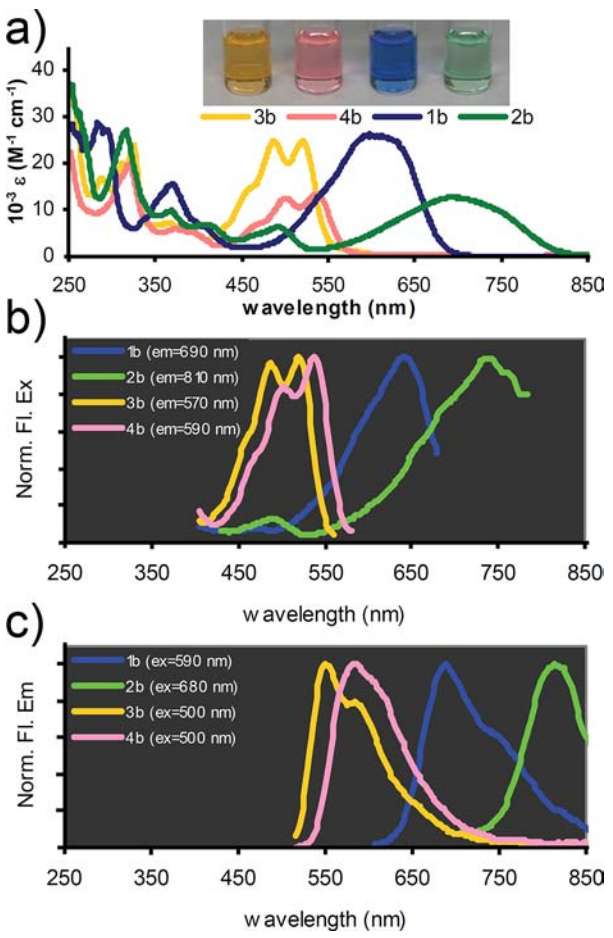

Figure 2. Absorption and fluorescence spectra of fully annulated **1b**, **2b**, and semiannulated **3b** and **4b** in MeOH. (a) Absorption. Insert: Room light Photograph of solutions in MeOH (left to right: **3b**, **4b**, **1b**, and **2b**). (b) Normalized fluorescence excitation spectra. (c) Normalized fluorescence emission spectra. Formal transposition of R_2 (Figure 1) modulates the HOMO−LUMO gap and shifts the absorption and fluorescence in both the symmetric (**1** and **2**) and asymmetric (**3** and **4**) pairs. Additional spectra in MeOH and DMSO are provided (Figures S31−S33 of the Supporting Information).

Table 1. Experimental and Calculated Spectral Properties of 1b−4b in MeOH

compound	$\lambda_{max\ abs}$ (nm)	$\lambda_{max\ em}$ (nm)	HOMO (eV)	LUMO (eV)	gap (eV)	$\lambda_{max\ abs}$ calcd (nm)
1b	598	688	−5.011	−2.719	−2.292	541
2b	701	816	−4.781	−2.688	−2.093	592
3b	487, 521	550	5.442	2.367	3.075	403
4b	501, 536	582	5.606	2.667	2.939	422

(part c of Figure 2) of **2b** and **4b** (128 and 32 nm as compared to **1b** and **3b**, respectively). Importantly, **2b** absorbs and emits in the near-infrared with absorption and emission maxima of 701 and 816 nm.[19] Analogous trends are observed in other solvent systems (below and Figure S34 of the Supporting Information). Spectral properties of these and other compounds from families **1**−**4** in other solvents are tabulated in Table S1 of the Supporting Information.

Induced Through-Space Interactions and Intramolecular Hydrogen Bonding. Although the red shift in the

dx.doi.org/10.1021/ja302445w | J. Am. Chem. Soc. 2012, 134, 10502−10508

absorption of **4b** in MeOH appears modest, its corresponding anion **4c** in DMSO:aqueous base 1:9 is shifted more substantially by 50 to 599 nm as compared to anion **3c** under the same conditions.[20] Its fluorescence emission is shifted by an even larger 130 nm emitting at 760 nm (as described below). The comparatively large shift of the anion **4c** further supports a polar effect as playing a key role in modulating the HOMO−LUMO gap. The oxoanion of asymmetric **4c** should have a more significant field effect on the polarity of the proximal ether oxygen as compared to the corresponding oxoanion **3c**.

There are through-space polar interactions between R_2 and the internal bridge oxygen in **4a−d**. In the case of symmetric **2a−d**, the field effect is further enhanced by the oxygen on C-13 (Figure 1). The relatively larger difference in absorption maxima of **2b** as compared to **1b** (part a of Figure 2) is also attributable at least in part to the unique intramolecular hydrogen bonding network present in **2b** (Figures 3 and 4).

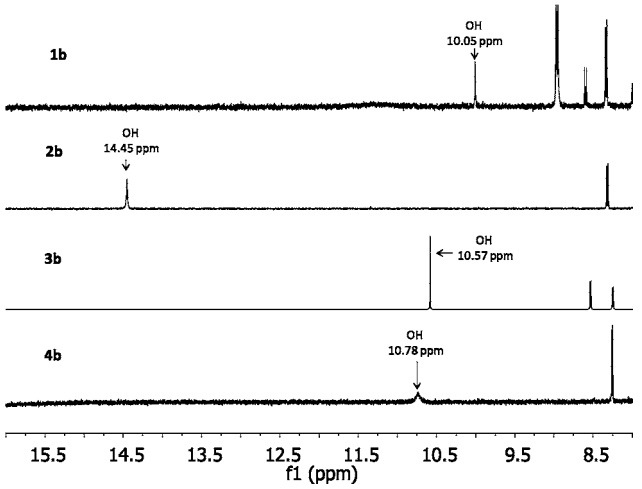

Figure 3. ^{1}H NMR spectra in DMSO-d_6 of **1b**, **2b**, **3b**, and **4b** showing the different chemical shifts observed for the hydroxyl protons.

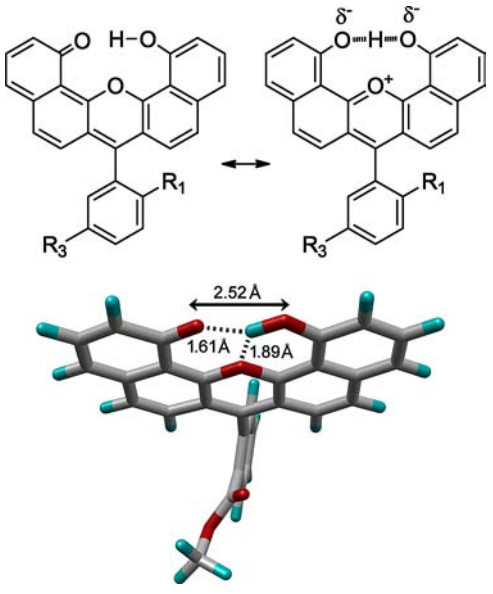

Figure 4. Hydrogen bond network of **2** and energy-minimized structure of **2b** showing how this enhances coplanarity of the fused ring system.

This network results in enhanced negative charge density on the ionizable oxygen atoms, thereby promoting a relatively large bathochromic shift, as in the analogous case of anionic **4c** described above.

Hydrogen bonding is evidenced in the ^{1}H NMR in DMSO-d_6 (Figure 3) and absorption spectra (Figure S35 of the Supporting Information) of **2b**. The shared proton resonates significantly downfield (14.45 ppm) as compared to the corresponding phenolic proton of **1b** (10.05 ppm). This strong deshielding can be attributed to a redistribution of the electronic density around the hydrogen atom that occurs upon hydrogen bond formation between the hydroxyl proton, the carbonyl, and the central oxygen of **2b**. Evidence of hydrogen bonding is also observed in **4b** but to a lesser degree. The hydrogen bonded proton is slightly downfield (10.78 ppm) as compared to the phenolic proton of **3b** (10.57 ppm). The strong deshielding observed for the hydroxyl proton of **2b** indicates that it is involved in the formation of a low barrier hydrogen bond (LBHB).[21] LBHBs play an important role in enzymatic processes[21a,22] as well as in supramolecular assemblies.[23]

In general, LBHBs have been observed in systems were the donor−acceptor distances are shorter than normal hydrogen bonds.[22c,24] In **2b**, simulations show that the total hydrogen bond distance O···H−O between the carbonyl and the hydroxyl at the C-1 position is 2.52 Å, which is lower than the typical hydrogen bonding distance O···H−O (≥2.8 Å) and close to the average distance observed for LBHBs (2.55 Å). In **4b**, the total hydrogen bond distance O···H−O between the hydroxyl at the C-1 position and the xanthene central oxygen is 2.95 Å, which falls in range of common hydrogen bonds.

As further evidence of the effect of the hydrogen bonding network on the characteristics of **2**, removal of the shared proton (under harsh conditions, 12.5 mM NaOH, to form **2c**) does not result in a large bathochromic shift in the absorption as is observed when **1b** is deprotonated to **1c** (Figure S36 of the Supporting Information). In addition, unlike conventional naphthofluorescein compounds in which the fluorescence is minimal for the protic species in aqueous solvents[9a,f] the protic species of family **2** is more fluorescent than the corresponding ionized chromophore. For example, NIR fluorescence was observed in family **2** compounds up to pH 9, whereas removal of the shared proton was observed to quench the fluorescence (Figures S37−38 of the Supporting Information). Molecular simulations demonstrate that the hydrogen bonding network enhances coplanarity of the fused ring system of compounds in family **2** (Figure 4 and Figure S39 of the Supporting Information).

Molecular Modeling. The bathochromic shifts in the absorption spectra induced through formal transposition (Figure 1, from C-3 to C-1) of the polar ionizable oxygen groups were evaluated by calculating the HOMO−LUMO energies of both the protic and anionic species and comparing the calculated absorbance maxima with experimental data in MeOH or DMSO:aqueous 1:9, respectively.[25] Molecular surfaces and energies are provided in Figures S40−50 of the Supporting Information and included for comparison with the spectral data in Table S1 of the Supporting Information. In general, modeling systematically underestimated the HOMO−LUMO gap (i.e., overestimated the absorption wavelength) of deprotonated species and overestimated the gap (i.e., underestimated the absorption wavelength) for protic species. However, in each case, bathochromic shifts were both predicted

and observed for compounds with formally transposed R groups (i.e., families **2** and **4** as compared to **1** and **3**, respectively). Figure 5 shows the calculated molecular surfaces

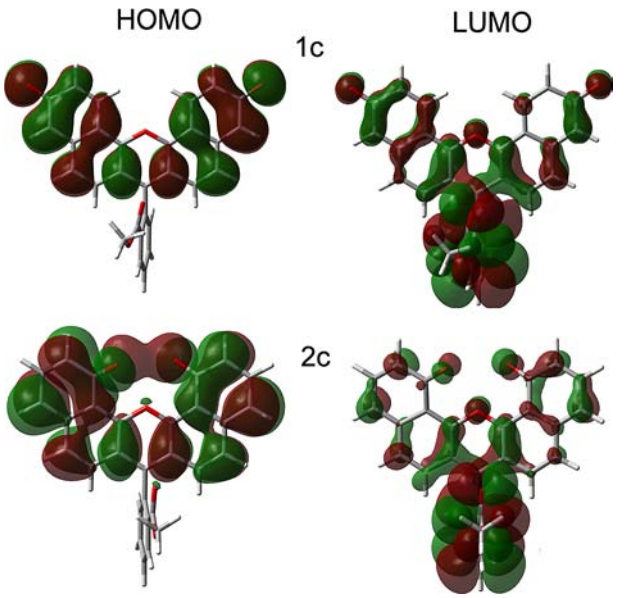

Figure 5. Calculated molecular surfaces of the HOMO and LUMO of **1c** and **2c** (basis set DFT B3LYP/6-31G).[29] Additional molecular surfaces for other compounds are provided in the Supporting Information.

of anions **1c** and **2c**. The results indicate that formal transposition effectively modulates the HOMO−LUMO gap. Molecular modeling most adequately predicts the magnitude of transposition-induced shifts for the deprotonated fully annulated compounds. When comparing **1c** and **2c**, the 73 nm calculated bathochromic shift is in agreement with the 79 nm observed experimental shift of **2c** as compared to **1c**. An experimental bathochromic shift of ∼50 nm (calculated shift of ∼90 nm) was observed for semiannulated anion **4c** as compared to **3c**. The modeling also reveals an unusual through-space overlap of the C-1 and C-13 oxygen orbitals in the HOMO of **2c** that result in homoconjugation of the π-system in the chromophore. For **2c**, the distance between the oxygens of C-1 and C-13 is 3.2 Å. Because the typical distance for a O−O bond is about 1.5 Å, this interaction could be involving variations of the molecular dipole moment through space. The five-membered fused-ring system in the **2** family is less planar in the anionic form due to the electrostatic repulsion of the oxygens of C-1 and C-13, and this allows the through-space overlapping of the oxygens' orbitals of the HOMO that would not be possible if the anionic form was planar (Figure 6).

Examples of other molecular architectures (restricted coplanarity featuring oxygen atoms relatively close in space)

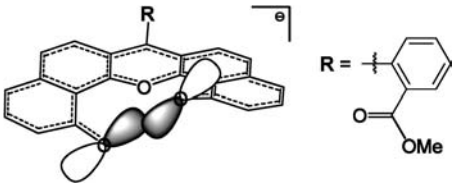

Figure 6. Overlapping of the molecular orbitals of the oxygens at C-1 and C-13 in **2c**.

similar to **2** include 1,1′-binaphthalene-2.2′-diol (binol)[26] and, more recently, HelMe, a [4]heterohelicene cation.[27] In binol, the positions of the oxygens are not restricted and therefore a direct comparison with **2c** is not possible. In the case of the [4]heterohelicene cation, HelMe (Figure 7) the oxygen atoms

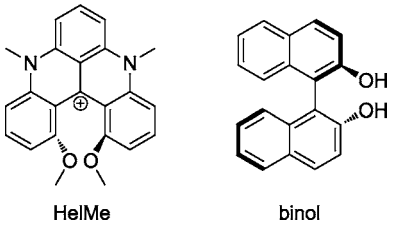

Figure 7. Known architectures positioning oxygen atoms relatively close in space.

seem to be forced to be close but the calculated molecular surfaces of the published HOMO do not show a through-space overlapping of the oxygens' orbitals as in the case of **2c**.[28]

The NIR absorbing properties of **2** render these compounds attractive. NIR absorbing compounds are widely used in areas such as optical recording, thermal-writing displays, laser printers, laser filters, infrared photography, photodynamic therapy, and many other applications including solar cells and heat absorbers.[30] A current limitation in the field of solar cells is the mismatch between the absorbing dye and the solar emission spectrum.[30b] Compound **2b** is NIR active in the solid state (Figure S51 of the Supporting Information) and the absorption spectra of **2b** and **2c** match well with the 690 nm maximum photon flux of sunlight.[30b]

The long-wavelength absorptions of the dyes in the **2** family suggest that they could be useful as dyes for solar cells given that a major goal for improvement of organic solar cells is improved absorption in the far red and NIR region.[31] In addition, the best dyes for dye-sensitized solar cells (DSSCs) use phenylcarboxylates as anchoring groups and have a donor−acceptor structure in which the HOMO is localized on the donor portion, whereas the LUMO is localized on the acceptor portion; this facilitates injection of the excited electron into the semiconductor (e.g., TiO_2) on which the dye is adsorbed.[32]

The electron density of the HOMO of **2c** (Figure 5) and **4c** is located nearly exclusively on the chromophore, whereas in the LUMO nearly all of the electron density is located on the lower ring containing the ester moiety. These striking electronic properties are unique to chromophores **2** and **4**, except, as expected, for **2d**, which contains electron donating groups on the lower arene. Enhanced electron density in the LUMO at the sight of attachment to the metal surface of a solar cell is critical for efficient electron transfer.

Spectroscopic Characterization in Aqueous Media. The unique absorption and fluorescence properties of protic species **2b** that arise from through space field effects and intramolecular hydrogen bonding, involving all three oxygens of the xanthene chromophore, were described above. Compounds **4a−d** possess enhanced spectral properties for applications including biological imaging and diagnostics wherein long wavelength activity is advantageous. Positioning the hydroxyl group on C-1, to afford a field effect between two polar atoms, the bridging xanthene oxygen, and the C-1 oxygen in the case of **4c**, was found to have a greater effect on the emission wavelength of **4c** than on the absorption as compared to **3c** (∼130 nm bathochromic shift in emission vs ∼50 nm shift in

dx.doi.org/10.1021/ja302445w | J. Am. Chem. Soc. 2012, 134, 10502−10508

absorption, as described above). The difference between these shifts results in NIR emission at 760 nm with a significantly enhanced Stokes shift of 160 nm. For comparison, the analogous long wavelength anionic form of commercial SNAFL-1 (**3a**) is reported to absorb and emit at 537 and 624 nm respectively with a comparatively modest Stokes shift of 87 nm and a quantum yield of 0.093.[9b] The Stokes shift of other xanthene dyes, that is fluorescein and rhodamine derivatives, is typically ∼20 nm. Note that, in the **1** and **3** series, field effects are not promoted due to the distal positioning of all three oxygens of the chromophore moiety.

Like many other NIR emitting compounds, **4c** displays a relatively low quantum yield (less than 1%) in aqueous solution. The fluorescence quantum yield of ICG is limited by internal conversion to only a few percent.[4] The brightness of **4c** is comparable to that of other novel NIR probes including carbon nanotubes,[33] which exhibit extinction coefficient[34] of approximately 4400 and low fluorescence efficiencies of typically <0.1%.[35] It is well known that the absence of interfering background increases the sensitivity of NIR fluorophores far beyond other visible dyes with much higher quantum yields.[36] Efforts to increase the quantum yield beyond that of other NIR emitting probes are underway.

We find that straightforward functionalization through methylation of the C-3 oxygen to afford methyl ether **4d** dramatically improves the quantum yield. The quantum yield of yellow-orange emitting **4d** is 0.4649, 40 times greater than the corresponding neutral **4b**. It is slightly higher than yellow-green emitting neutral **3b** and >2 times higher than orange-red emitting anion **3c** (Figure 8). Formal transposition of the

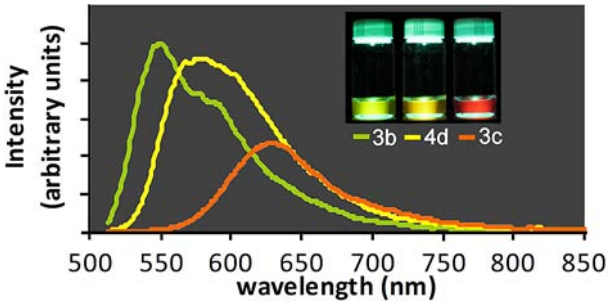

Figure 8. Fluorescence emission spectra of **3b**, **3c**, and methyl ether **4d** in 10:90 DMSO:aqueous. Solutions were prepared such that the absorbances at the 500 nm excitation wavelength were equal for all solutions. Insert: Fluorescence emission in a darkened room of 7.5 μM solutions (**3b**, **4d**, and **3c** from left to right) excited from below with 3-W megaMAX 505 nm ALS system. Neutral **3b** is in pH 6 phosphate buffer, 12.5 mM, whereas anion **3c** is in pH 12 NaOH. Compound **4d** is in pH 7.4 phosphate buffer, 12.5 mM.

hydroxyl moiety (Figure 1) shifts the spectral properties such that the short wavelength forms of these compounds (**4b** and **4d**) are redder than the short wavelength forms and approach the long wavelength forms of known seminaphthofluorescein probes (for example **3a** and its analogues, i.e. carboxy SNAFL-1 including an additional carboxylate group on the lower ring). The emission enhancing properties afforded through the combination of formal transposition with methylation is in contrast to previously reported methyl ethers of seminaphthofluorescein compounds lacking such enhancement.[9b] Interestingly, methylation of **4b** results in only **4d** (exhaustive attempts to synthesize the corresponding isomer of **4d**, where the substituents on C-1 and C-10 are interchanged were unsuccessful, as seen in Scheme S1 of the Supporting Information). The quantum yield of **4d** is ∼1.5 times greater than the short wavelength emitting methyl ether of carboxy SNAFL-1 in which the C-3 oxygen was methylated, and ∼15 times greater than the analogous red-emitting C-10 methyl ether.[9b] Thus, methylation of **4b** affords pH independent and relatively brighter red fluorescence compared to known seminaphthofluorescein probes.

CONCLUSIONS

In summary, the results described herein demonstrate that xanthene dye absorption and emission can be shifted to the NIR via relatively simple structural (e.g., regioisomeric) changes involving field effects or low barrier hydrogen bonds depending on the ionization of the chromphore. This design principle, involving the environment of the bridging ether oxygen, apparently allows for favorable modulation of the HOMO−LUMO gap. Large Stokes shifts are observed as well as an enhancement in quantum yield and brightness as compared to analogous known long wavelength emitting dyes. Ongoing efforts in our laboratory include the study of related field effects on rhodols, rhodamines, and other xanthenes, as well as other chromophores.

EXPERIMENTAL SECTION

Chemistry. Unless otherwise indicated, all commercially available starting materials were used directly without further purification. Silica gel Sorbent Technologies 32−63 μm was used for flash column chromatography. ^{1}H- and ^{13}C NMR were obtained on either a ARX-400 or ARX 600 Advance Bruker spectrometer. Chemical shifts (δ) are given in ppm relative to DMSO-d_6 (2.50 ppm, ^{1}H, 39.52 ^{13}C) unless otherwise indicated. MS (HRMS, ESI) spectra were obtained at the PSU Bioanalytical Mass Spectrometry Facility on a Thermo-Electron LTQ-Orbitrap high resolution mass spectrometer with a dedicated Accela HPLC system. 1,8-dihydroxynaphthalene and 2-(2,4-dihydroxybenzoyl)-benzoic acid were synthesized as described in the literature.[16,9a,17]

Crystallographic Data for 4a. $C_{24}H_{14}O_5$, monoclinic space group $C2/c$, a = 19.5457(15), b = 12.2406(10), c = 15.4763(14) Å, β = 114.233(5)°, V = 3376.5(5) Å^3, Z = 8, ρ_{calcd} = 1.504 g cm^{-3}, μ(CuKα) = 0.87 mm^{-1}, R = 0.033 for 2667 data with $F_o^2 > 2\sigma(F_o^2)$ of 3070 unique data and 269 refined parameters. A total of 13 499 data (R_{int} = 0.031) was collected at T = 90.0(5) K to θ = 68.9° with CuKα radiation (λ = 1.54178 Å) on a Bruker Kappa Apex II diffractometer, using an amber crystal of dimensions 0.11 × 0.13 × 0.17 mm. Refinement was by full-matrix least-squares using SHELXL, with H atoms in idealized positions, except for OH hydrogen atoms, which were located by difference maps and their positions refined.

UV−vis and Fluorescence Measurements. Absorbance spectra were collected on a Cary 50 UV−vis spectrophotometer. Fluorescence spectra were collected on a Cary Eclipse fluorescence spectrophotometer (Agilent Technologies). All absorbance spectra were reference corrected. Fluorescence spectra were corrected for the wavelength dependent response of the R928 photomultiplier tube using a manufacturer generated correction file. Quantum yields are reported as the average of multiple measurements using multiple references. Red emitting probes were referenced to rhodamine 101

(0.913)[37] and sulforhodamine 101 (0.900)[38] in EtOH. NIR emitting probes were referenced to Nile Blue (0.27),[39] IR-125 (0.132),[37] and HEDITCP (0.195)[37] in EtOH. HEDITCP was prepared as reported by Descalzo.[40] Concentrations were adjusted such that absorbance values were ~0.05 or lower. Differences in refractive index between sample and solution were accounted for.

Molecular Modeling. molecular orbital calculations were performed using the Density functional theory (DFT) at B3LYP/6-31G level using *Gaussian 03W*.

■ ASSOCIATED CONTENT

Ⓢ Supporting Information

Detailed experimental procedures, synthesis, spectral and characterization data. Crystallographic data for **4a** (as the lactone form). This material is available free of charge via the Internet at http://pubs.acs.org.

■ AUTHOR INFORMATION

Corresponding Author

*E-mail: strongin@pdx.edu

Notes

The authors declare no competing financial interest.

■ ACKNOWLEDGMENTS

The authors thank Dr. Carl Wamser for valuable discussions. This work was supported by the National Institutes of Health (RO1 EB002044) and the NSF (Grant 0741993) for the purchase of the LTQ-Orbitrap Discovery.

■ ABBREVIATIONS

DMF, dimethyl formamide; DMSO, dimethylsulfoxide; DSSCs, dye-sensitized solar cells; ESI, electrospray ionization; FDA, Food and Drug Administration; HEDITCP, 1,10,3,3,30,30-hexamethyl-3,5-ethylene-4-(dimethylamino)-2,20-indotricarbocyanine perchlorate; HelMe, 1,13-dimethoxy-5,9-dimethyl-5,9-dihydroquinolino[2,3,4-kl]acridin-13b-ylium; HPDITCP, 1,10,3,3,30,30-hexamethyl-3,5-propylene-4-(dimethylamino)-2,20-indotricarbocyanine perchlorate; HOMO, highest occupied molecular orbital; HRMS, high resolution mass spectrometry; ICG, indocyanine green; LBHB, low-barrier hydrogen bond; LUMO, lowest unoccupied molecular orbital; NIR, near-infrared; SNAFL, seminaphthofluorescein; TFA, trifluoroacetic acid

■ REFERENCES

(1) Escobedo, J. O.; Rusin, O.; Lim, S.; Strongin, R. M. *Curr. Opin. Chem. Biol.* **2010**, *14*, 64.

(2) Alford, R.; Simpson, H. M.; Duberman, J.; Hill, G. C.; Ogawa, M.; Regino, C.; Kobayashi, H.; Choyke, P. L. *Mol. Imaging* **2009**, *8*, 341.

(3) Ogawa, M.; Kosaka, N.; Choyke, P. L.; Kobayashi, H. *Cancer Res.* **2009**, *69*, 1268.

(4) Philip, R.; Penzkofer, A.; Baumler, W.; Szeimies, R. M.; Abels, C. *J. Photochem. Photobiol., A* **1996**, *96*, 137.

(5) (a) Mizutani, T. *J. Environ. Public Health* **2009**, *2009*, Article ID 953952. (b) Lipman, A. L. Safety of xanthene dyes according to the US Food and Drug Administration. In *Light-Activated Pest Control*; Heitz, J. R., Downum, K. R., Eds.; American Chemical Society: WA, 1995; Vol. *616*, p 34.

(6) (a) Haley, N. F. *J. Heterocycl. Chem.* **1977**, *14*, 683. (b) Shi, J. M.; Zhang, X. P.; Neckers, D. C. *Tetrahedron Lett.* **1993**, *34*, 6013.

(7) (a) Sauer, M.; Han, K.-T.; Muller, R.; Nord, S.; Schulz, A.; Seeger, S.; Wolfrum, J.; Arden-Jacob, J.; Deltau, G.; Marx, N. J.; Zander, C.; Drexhage, K. H. *J. Fluoresc.* **1995**, *5*, 247. (b) Liu, J. X.; Diwu, Z. J.; Leung, W. Y.; Lu, Y. X.; Patch, B.; Haugland, R. P. *Tetrahedron Lett.* **2003**, *44*, 4355.

(8) (a) Arden-Jacob, J.; Frantzeskos, J.; Kemnitzer, N. U.; Zilles, A.; Drexhage, K. H. *Spectroc. Acta Pt. A-Molec. Biomolec. Spectr.* **2001**, *57*, 2271. (b) Kolmakov, K.; Belov, V. N.; Wurm, C. A.; Harke, B.; Leutenegger, M.; Eggeling, C.; Hell, S. W. *Eur. J. Org. Chem.* **2010**, 3593.

(9) (a) Lee, L. G.; Berry, G. M.; Chen, C. H. *Cytometry* **1989**, *10*, 151. (b) Whitaker, J. E.; Haugland, R. P.; Prendergast, F. G. *Anal. Biochem.* **1991**, *194*, 330. (c) Fabian, W. M. F.; Schuppler, S.; Wolfbeis, O. S. *J. Chem. Soc., Perkin Trans. 2* **1996**, 853. (d) Chang, C. J.; Jaworski, J.; Nolan, E. M.; Sheng, M.; Lippard, S. J. *Proc. Natl. Acad. Sci. U. S. A.* **2004**, *101*, 1129. (e) Furukawa, K.; Abe, H.; Wang, J.; Uda, M.; Koshino, H.; Tsuneda, S.; Ito, Y. *Org. Biomol. Chem.* **2009**, *7*, 671. (f) Azuma, E.; Nakamura, N.; Kuramochi, K.; Sasamori, T.; Tokitoh, N.; Sagami, I.; Tsubaki, K. *J. Org. Chem.* **2012**, *77*, 3492. (g) Sibrian-Vazquez, M.; Escobedo, J. O.; Lowry, M.; Strongin, R. M. *Pure Appl. Chem.* **2012**, DOI: 10.1351/pac-con-11-11-06.

(10) Fu, M. Y.; Xiao, Y.; Qian, X. H.; Zhao, D. F.; Xu, Y. F. *Chem. Commun.* **2008**, 1780.

(11) (a) Yamashita, Y.; Ono, K.; Tomura, M.; Tanaka, S. *Tetrahedron* **1997**, *53*, 10169. (b) Aouchiche, H. A.; Djennane, S.; Boucekkine, A. *Synth. Met.* **2004**, *140*, 127.

(12) Qian, X. H.; Xiao, Y.; Xu, Y. F.; Guo, X. F.; Qian, J. H.; Zhu, W. P. *Chem. Commun.* **2010**, *46*, 6418.

(13) Egawa, T.; Koide, Y.; Hanaoka, K.; Komatsu, T.; Terai, T.; Nagano, T. *Chem. Commun.* **2011**, *47*, 4162.

(14) (a) Egawa, T.; Hanaoka, K.; Koide, Y.; Ujita, S.; Takahashi, N.; Ikegaya, Y.; Matsuki, N.; Terai, T.; Ueno, T.; Komatsu, T.; Nagano, T. *J. Am. Chem. Soc.* **2011**, *133*, 14157. (b) Koide, Y.; Urano, Y.; Hanaoka, K.; Terai, T.; Nagano, T. *ACS Chem. Biol.* **2011**, *6*, 600. (c) Koide, Y.; Urano, Y.; Hanaoka, K.; Terai, T.; Nagano, T. *J. Am. Chem. Soc.* **2011**, *133*, 5680. (d) Koide, Y.; Urano, Y.; Hanaoka, K.; Piao, W.; Kusakabe, M.; Saito, N.; Terai, T.; Okabe, T.; Nagano, T. *J. Am. Chem. Soc.* **2012**, *134*, 5029.

(15) McNaugth, A. D.; Wilkinson, A. *IUPAC. Compendium of Chemical Terminology (the "Gold Book")*, 2nd ed.; Blackwell Scientific Publications: Oxford, 1997.

(16) Yang, Y. J.; Lowry, M.; Xu, X. Y.; Escobedo, J. O.; Sibrian-Vazquez, M.; Wong, L.; Schowalter, C. M.; Jensen, T. J.; Fronczek, F. R.; Warner, I. M.; Strongin, R. M. *Proc. Natl. Acad. Sci. U. S. A.* **2008**, *105*, 8829.

(17) (a) Arnoldi, A.; Bassoli, A.; Borgonovo, G.; Merlini, L.; Morini, G. *J. Agric. Food. Chem.* **1997**, *45*, 2047. (b) Wada, K.; Fujita, T.; Ogawa, Y.; Koda, T.; Aoki, H. *Food Addit. Contam.* **2004**, *21*, 1137. (c) Wei, B. L.; Wu, S. H.; Chung, M. I.; Won, S. J.; Lin, C. N. *Eur. J. Med. Chem.* **2000**, *35*, 1089.

(18) Han, J. Y.; Burgess, K. *Chem. Rev.* **2010**, *110*, 2709.

(19) The emission of **2b** extends well beyond the working range of our instrument (Figure 2). Its quantum yield is estimated to be on the order of ~0.1% (Table S1 of the Supporting Information), comparable to other extended xanthenes.[9f]

(20) New methyl ester analogues of known **1a** and **3a** (e.g., anions **1c** and **3c**) display similar properties to the known compounds upon deprotonation; differing by a small 5−10 nm bathochromic shift and elimination of the carboxylate-lactone equilibrium (Table S1 of the Supporting Information).

(21) (a) Cleland, W. W.; Kreevoy, M. M. *Science* **1994**, *264*, 1887. (b) Pacios, L. F.; Gomez, P. C. *J. Phys. Chem. A* **2004**, *108*, 11783.

(22) (a) Frey, P. A.; Whitt, S. A.; Tobin, J. B. *Science* **1994**, *264*, 1927. (b) Marx, D.; Tuckerman, M. E.; Hutter, J.; Parrinello, M. *Nature* **1999**, *397*, 601. (c) Schiott, B.; Iversen, B. B.; Madsen, G. K. H.; Larsen, F. K.; Bruice, T. C. *Proc. Natl. Acad. Sci. U. S. A.* **1998**, *95*, 12799.

(23) (a) Basu, A.; Das, G. *CrystEngComm* **2012**, *14*, 3306. (b) Day, V. W.; Hossain, A.; Kang, S. O.; Powell, D.; Lushington, G.; Bowman-James, K. *J. Am. Chem. Soc.* **2007**, *129*, 8692. (c) Kadarkaraisamy, M.; Caple, G.; Gorden, A. R.; Squire, M. A.; Sykes, A. G. *Inorg. Chem.* **2008**, *47*, 11644. (d) Kolonko, K. J.; Reich, H. J. *J. Am. Chem. Soc.*

2008, *130*, 9668. (e) Pozharskii, A. F.; Degtyarev, A. V.; Ozeryanskii, V. A.; Ryabtsova, O. V.; Starikova, Z. A.; Borodkin, G. S. *J. Org. Chem.* **2010**, *75*, 4706.
(24) Grabowski, S. J. *Chem. Rev.* **2011**, *111*, 2597.
(25) Figure S34 and Table S1 of the Supporting Information and associated discussion.
(26) Pummerer, R.; Prell, E.; Rieche, A. *Chem. Ber.* **1926**, *59*, 2159.
(27) Herse, C.; Bas, D.; Krebs, F. C.; Bürgi, T.; Weber, J.; Wesolowski, T.; Laursen, B. W.; Lacour, J. *Angew. Chem., Int. Ed.* **2003**, *42*, 3162.
(28) Kel, O.; Sherin, P.; Mehanna, N.; Laleu, B.; Lacour, J.; Vauthey, E. *Photochem. Photobiol. Sci.* **2012**, *11*, 623.
(29) Frisch, M. J.; Trucks, G. W.; Schlegel, H. B.; Scuseria, G. E.; Robb, M. A.; Cheeseman, J. R.; Montgomery, J., J. A.; Vreven, T.; Kudin, K. N.; Burant, J. C.; Millam, J. M.; Iyengar, S. S.; Tomasi, J.; Barone, V.; Mennucci, B.; Cossi, M.; Scalmani, G.; Rega, N.; Petersson, G. A.; Nakatsuji, H.; Hada, M.; Ehara, M.; Toyota, K.; Fukuda, R.; Hasegawa, J.; Ishida, M.; Nakajima, T.; Honda, Y.; Kitao, O.; Nakai, H.; Klene, M.; Li, X.; Knox, J. E.; Hratchian, H. P.; Cross, J. B.; Bakken, V.; Adamo, C.; Jaramillo, J.; Gomperts, R.; Stratmann, R. E.; Yazyev, O.; Austin, A. J.; Cammi, R.; Pomelli, C.; Ochterski, J. W.; Ayala, P. Y.; Morokuma, K.; Voth, G. A.; Salvador, P.; Dannenberg, J. J.; Zakrzewski, V. G.; Dapprich, S.; Daniels, A. D.; Strain, M. C.; Farkas, O.; Malick, D. K.; Rabuck, A. D.; Raghavachari, K.; Foresman, J. B.; Ortiz, J. V.; Cui, Q.; Baboul, A. G.; Clifford, S.; Cioslowski, J.; Stefanov, B. B.; Liu, G.; Liashenko, A.; Piskorz, P.; Komaromi, I.; Martin, R. L.; Fox, D. J.; Keith, T.; Al-Laham, M. A.; Peng, C. Y.; Nanayakkara, A.; Challacombe, M.; Gill, P. M. W.; Johnson, B.; Chen, W.; Wong, M. W.; Gonzalez, C.; Pople, J. A. Gaussian, Inc., Wallingford CT, 2004.
(30) (a) Fabian, J.; Nakazumi, H.; Matsuoka, M. *Chem. Rev.* **1992**, *92*, 1197. (b) Qian, G.; Wang, Z. Y. *Chem. Asian J.* **2010**, *5*, 1006.
(31) Ameri, T.; Dennler, G.; Lungenschmied, C.; Brabec, C. J. *Energy Environ. Sci.* **2009**, *2*, 347.
(32) (a) Walter, M. G.; Rudine, A. B.; Wamser, C. C. *J. Porphyrins Phthalocyanines* **2010**, *14*, 759. (b) Yella, A.; Lee, H. W.; Tsao, H. N.; Yi, C. Y.; Chandiran, A. K.; Nazeeruddin, M. K.; Diau, E. W. G.; Yeh, C. Y.; Zakeeruddin, S. M.; Gratzel, M. *Science* **2011**, *334*, 629.
(33) Boghossian, A. A.; Zhang, J. Q.; Barone, P. W.; Reuel, N. F.; Kim, J. H.; Heller, D. A.; Ahn, J. H.; Hilmer, A. J.; Rwei, A.; Arkalgud, J. R.; Zhang, C. T.; Strano, M. S. *Chemsuschem* **2011**, *4*, 848.
(34) Schoppler, F.; Mann, C.; Hain, T. C.; Neubauer, F. M.; Privitera, G.; Bonaccorso, F.; Chu, D. P.; Ferrari, A. C.; Hertel, T. *J. Phys. Chem. C* **2011**, *115*, 14682.
(35) Lee, A. J.; Wang, X. Y.; Carlson, L. J.; Smyder, J. A.; Loesch, B.; Tu, X. M.; Zheng, M.; Krauss, T. D. *Nano Lett.* **2011**, *11*, 1636.
(36) Raghavachari, R. Introduction. In *Near-Infrared Applications in Biotechnology*; Raghavachari, R., Ed.; Marcel Dekker, Inc.: New York, NY, 2001, p 1.
(37) Rurack, K.; Spieles, M. *Anal. Chem.* **2011**, *83*, 1232.
(38) Birge; R. R. Kodak Laser Dyes, Vol. JJ-169, Eastman Kodak Company: Rochester, NY, 1987.
(39) Sens, R.; Drexhage, K. H. *J. Lumin.* **1981**, *24*−*5*, 709.
(40) Descalzo, A. B.; Rurack, K. *Chem.—Eur. J.* **2009**, *15*, 3173.